

The Preliminary CatWISE Catalog: Motions from *WISE* and *NEOWISE* Data

PETER R. M. EISENHARDT,¹ FEDERICO MAROCCHI,^{1,*} JOHN W. FOWLER,² NELSON GARCIA,³
THOMAS H. JARRETT,⁴ J. DAVY KIRKPATRICK,³ RENATA KOONTZ,⁵ ELIJAH J. MARCHESE,⁵
AARON MEISNER,⁶ S. ADAM STANFORD,⁷ DAN CASELDEN,⁸ MICHAEL C. CUSHING,⁹ ROC M. CUTRI,³
JACQUELINE K. FAHERTY,¹⁰ CHRISTOPHER R. GELINO,³ ANTHONY H. GONZALEZ,¹¹
AMANDA MAINZER,¹ BAHRAM MOBASHER,⁵ DAVID J. SCHLEGEL,¹² DANIEL STERN,¹
HARRY I. TEPLITZ,³ AND EDWARD L. WRIGHT¹³

¹*Jet Propulsion Laboratory, California Institute of Technology, 4800 Oak Grove Drive, M/S 169-327, Pasadena, CA 91109, USA*

²*230 Pacific St., Apt. 205, Santa Monica, CA 90405 USA*

³*IPAC, Mail Code 100-22, Caltech, 1200 E. California Blvd., Pasadena, CA 91125, USA*

⁴*Department of Astronomy, University of Cape Town, Private Bag X3, Rondebosch, 7701, South Africa*

⁵*University of California, Riverside, 900 University Ave, Riverside, CA 92521*

⁶*National Optical Astronomy Observatory, 950 N. Cherry Ave., Tucson, AZ 85719, USA*

⁷*Department of Physics, University of California Davis, One Shields Avenue, Davis, CA 95616, USA*

⁸*Backyard Worlds, Moraga, CA, USA*

⁹*Department of Physics and Astronomy, University of Toledo, 2801 West Bancroft St., Toledo, OH 43606, USA*

¹⁰*American Museum of Natural History*

¹¹*University of Florida*

¹²*Lawrence Berkeley National Laboratory, Berkeley, CA, 94720, USA*

¹³*Department of Physics and Astronomy, UCLA, 430 Portola Plaza, Box 951547, Los Angeles, CA 90095-1547, USA*

(Revised May 15, 2019)

Submitted to

Corresponding author: Peter R. M. Eisenhardt. To be submitted to the Astronomical Journal.
Peter.R.Eisenhardt@jpl.nasa.gov

ABSTRACT

The Preliminary CatWISE catalog consists of 957,285,574 sources over the entire sky selected from *WISE* and *NEOWISE* survey data at 3.4 and 4.6 μm (W1 and W2) collected from 2010 to 2016. This dataset represents four times as many exposures and spans over ten times as large a time baseline as that used for the AllWISE catalog. CatWISE adapts AllWISE software to measure the sources in co-added images created from six month subsets of these data, each representing one coverage of the inertial sky, or epoch. The catalog includes the measured motion of sources in 8 epochs over the 6 year span of the data. From comparison to *Spitzer*, the SNR 5 Vega magnitude limits are W1=17.58 and W2=16.43, vs. W1=16.90 and W2=15.95 for AllWISE. From comparison to *Gaia*, the motions are an order of magnitude more accurate than those from AllWISE. The catalog is available to the astrophysics community at <https://catwise.github.io>.

Keywords: catalogs

1. INTRODUCTION

NASA’s Wide-field Infrared Survey Explorer mission (*WISE*; Wright et al. 2010) revealed iconic objects, including the first Earth Trojan asteroid (Connors et al. 2011), the closest and coolest brown dwarfs (Luhman 2013, 2014), and the most luminous galaxy yet found in the Universe (Tsai et al. 2015). These discoveries were made using two or more infrared coverages of the sky (or epochs) obtained from January 2010 to February 2011. Each epoch typically consists of a dozen exposures taken within two days at a given position. The satellite was reactivated as *NEOWISE* and resumed searching for near Earth objects in December 2013 (Mainzer et al. 2014), and has continued to cover the sky every six months since then.

* NASA Postdoctoral Program Fellow

In November 2013, the AllWISE release (Cutri et al. 2013) made available to the community an atlas from coadding the two dozen exposures from the initial year of WISE surveying, and a catalog of source fluxes and positions measured from those exposures. With at least two epochs per inertial position, AllWISE also provided motion estimates, and became the definitive catalog in the WISE bandpasses. Each year, *NEOWISE* releases the individual exposures from the reactivated survey (Cutri et al. 2015), corresponding to two additional epochs. With the 2019 April 10 *NEOWISE* release, exposures from 12 epochs, each of which has a dozen or more exposures at a given position, are now available. Meisner et al. (2018a) produced an image atlas which combines the 2010 and 2011 used for AllWISE with the 2013 through 2016 *NEOWISE* data. An obvious next step is to catalog the sources revealed in these combined exposures.

The unWISE catalog (Schlafly et al. 2019) uses a crowded-field point-source photometry code called “crowdsource” to do this, measuring source fluxes and positions in the coadded image, with the measurements at $3.4\text{ }\mu\text{m}$ (W1) and $4.6\text{ }\mu\text{m}$ (W2) carried out independently. In contrast, CatWISE has adapted AllWISE software to produce a full sky catalog of sources selected simultaneously in both W1 and W2, and also provides motion estimates. CatWISE sources in the Preliminary catalog were selected from the ensemble of 8 epochs of *WISE* and *NEOWISE* data from Meisner et al. (2018a, the “full coadd”), and the least-squares best-fit solution for point source flux, position and motion were determined from measurements on the individual “epoch coadd” images (Meisner et al. 2018c). Because the total time between CatWISE epochs is over 6 years, compared to a typical value of 6 months for AllWISE, the CatWISE motion estimates are far more accurate. This plus the greater depth of the CatWISE catalog relative to AllWISE are being used to extend the census of the coldest brown dwarfs in the solar neighborhood and enable definitive measurement of the form of the low-mass end of the star formation process.

In §2 of the paper we summarize relevant aspects of the *WISE* and *NEOWISE* mission phases. §3 describes the CatWISE processing steps. §4 assesses the astrometric and photometric performance of CatWISE using comparisons to *Gaia* and *Spitzer* data. §5 provides some initial examples of science results enabled by CatWISE, and §6 provides information on accessing CatWISE data products.

2. OBSERVATIONS

WISE was launched on 2009 December 14, with its 40-cm telescope cooled to 12 K by an outer cryostat tank, and the W1 and W2 detectors operated at 32 K. The 12 and 22 μm (W3 and W4) detectors were cooled to 7.8 K by an inner cryostat tank. Both tanks were filled with frozen hydrogen. The cryostat cover was ejected and the first images obtained on 2009 December 31, and science survey data began being taken on 2010 January 7.

The full cryogenic survey covered the sky 1.2 times, continuing until the hydrogen in the outer tank evaporated on 2010 August 6. *WISE* then surveyed an additional 30% of the sky during its 3-Band (W1, W2, and W3) cryo phase, with the W3 detector operating at reduced sensitivity. After the cryogen in both tanks was exhausted on 2010 September 29, the post-cryogenic *NEOWISE* survey (Mainzer et al. 2011) in W1 and W2 began, as the telescope and detectors warmed to ~ 73 K. Surveying continued until 2011 February 1, completing a second pass over the sky in W1 and W2, after which the satellite was placed into hibernation. In September 2013, the spacecraft was brought out of hibernation, where it had equilibrated at ~ 200 K due to thermal radiation from the Earth, and renamed *NEOWISE*. On 2013 December 13, with the telescope and detectors passively cooled below 76 K, *NEOWISE* resumed surveying the sky every 6 months in W1 and (Mainzer et al. 2014).

The Preliminary CatWISE catalog is based on the combination of W1 and W2 exposures in the two sky coverages used for the AllWISE data release (Cutri et al. 2013) and in the six sky coverages from the 2017 *NEOWISE* data release. We use MJD 55480 (2010 Oct. 11) as the dividing point between cryogenic and post-cryogenic data. The average observation date is closer to MJD 56700 (2014 Feb. 12), which we adopt as the epoch for reporting positions when solving for source motion in the Preliminary catalog. Source positions, whether incorporating source motion or not, are given in the equinox J2000 coordinate frame.

3. CATWISE PROCESSING

CatWISE adapts the AllWISE pipeline to detect and measure source fluxes in the combined WISE and NEOWISE images provided by unWISE. A full description of the AllWISE pipeline is provided in [Cutri et al. \(2013\)](#).

CatWISE processing works in the J2000 coordinate footprint established by the WISE All-Sky Release, dividing the inertial sky into 18,240 overlapping square images (tiles), each approximately 1.56 deg on a side, aligned with the local right ascension and declination. Processing steps were carried out independently on each tile. For the Preliminary catalog, CatWISE uses the full depth unWISE coaddition of 8 epochs ([Meisner et al. 2018a](#)), and the 8 individual unWISE epoch coadds ([Meisner et al. 2018c](#), after astrometric modifications described below). Source detection was done on the full depth coadds, and source properties determined from measurements on the epoch coadds. Potential artifacts affecting the sources were identified, and sources in the tile overlap region were flagged to indicate which set of measurements from the multiple tiles should be used. Finally, sources were selected for inclusion in the catalog or reject files. We describe these steps in more detail below.

3.1. *unWISE Coadds*

The coadded images in the atlas released with the AllWISE (and All-Sky) catalogs were primarily intended to facilitate source detection, and for this reason they were convolved with the WISE PSF. The unWISE coadds [Lang \(2014\)](#) retain the resolution of individual WISE exposures. For source detection (§3.3) in the Preliminary CatWISE catalog, we convolved the full-depth unWISE coadds ([Meisner et al. 2018a](#)) with the PSF (§3.2), while for source measurement we used unWISE epoch coadds ([Meisner et al. 2018c](#)) without convolution. For uncertainties, the “std” unWISE images were used, which are the standard deviation at each pixel of the individual WISE exposures.

In order to be consistent with the *NEOWISE* astrometric system in the individual exposures used for post-hibernation unWISE coadds, the released individual pre-hibernation exposures used for AllWISE had to be corrected to the astrometric system used for *NEOWISE* images. All are tied to 2MASS, but while the AllWISE catalog includes corrections for the motions of the 2MASS reference

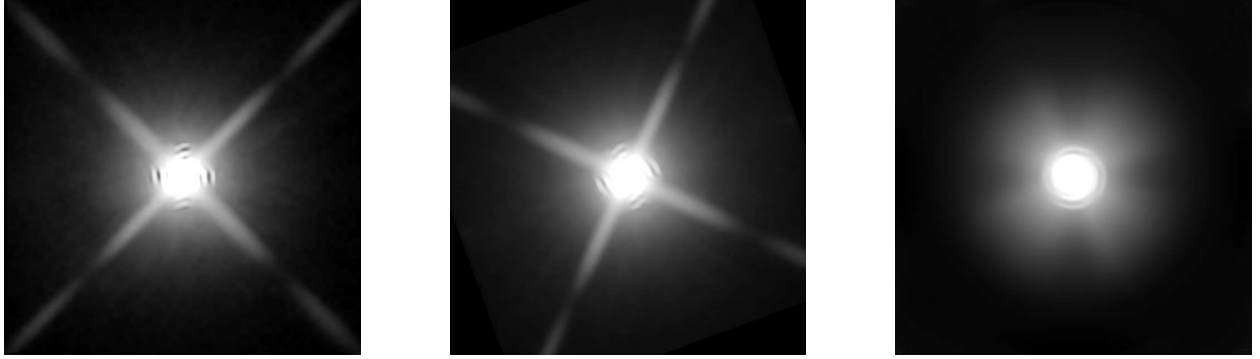


Figure 1. **Left:** Averaged post-cryogenic PSF model for W1. The grey scale uses a log stretch from 1% to 99% of the peak value. **Center:** The W1 PSF after averaging over cryo and post-cryogenic epochs, a PA range from 20.1397 to 20.3397 deg, and the ascending and descending scan directions. **Right:** An ascending-scan W1 PSF averaged over all epochs for tile 0890m667, which includes the south ecliptic pole and has a PA range from 235.13 to 306.82 deg.

stars as described in section V.2.b of the AllWISE Explanatory Supplement (Cutri et al. 2013), as do the *NEOWISE* images, the released pre-hibernation images do not. A table of corrections for these images exists, however ¹, and these corrections were applied to the unWISE input, making the astrometric system of the pre-hibernation epoch coadds consistent with those from the post-hibernation epoch coadds.

3.2. PSF

While much more stable than ground-based PSFs, the W1 and W2 PSFs vary with position in the focal plane, and changed somewhat between the cryogenic and post-cryogenic phases of the mission, particularly for W1. Model PSFs in a 9×9 grid over the focal plane for the cryo mission can be found in section IV.4.c.iii.1 of the WISE All-Sky Explanatory Supplement (Cutri et al. 2012), while the post-cryogenic PSFs used for NEOWISE are given in section IV.2.b.i of the NEOWISE Explanatory Supplement (Cutri et al. 2015).

¹ http://wise2.ipac.caltech.edu/docs/doc_tree/sis/rex19

CatWISE averages these model PSFs, weighted only by their partition sizes in the 9×9 array, since many focal plane positions contribute to the coadded images. Figure 1 (left) shows the resulting focal plane average post-cryogenic PSF model for W1.

The PSF is asymmetric (§3.2.1), with an orientation that is always the same in the WISE focal plane. The focal plane is closely aligned with the local ecliptic coordinate directions because of the WISE scanning strategy. The coadded image tile orientation is aligned with the local equatorial coordinate directions. It is therefore necessary to rotate the PSF model by the position angle (PA) between ecliptic and equatorial coordinates for each image tile.

The coadded images include a range of PA values, so a histogram of PA values is computed, using a bin width of 0.1 degrees. The basic PSF is rotated by each PA bin center value and averaged with weights equal to the histogram bin count. Tiles in the vicinity of the ecliptic poles have large PA ranges, and so the PSF becomes very smeared (see Figure 1 (right)). The PA averaging is done separately for cryo and post-cryogenic PSFs, and those averages are then combined for each tile with weights given by the number of corresponding epochs. The approach of processing all unWISE epoch images of a tile together in the photometry/astrometry step is referred to as option 0.

3.2.1. Asymmetry relative to scan direction

The WISE survey pattern covers the same region of inertial sky every six months, but because this occurs on opposite sides of the WISE orbit, the direction of the survey scan alternates between ascending and descending in ecliptic latitude. The WISE PSFs contain fine structure in the core that is far from being rotationally symmetric. Figure 2 shows the difference between ascending and descending orientations of the W1 post-cryogenic PSF. The bright and dark stripes in and around the core correspond to variations of almost a factor of two. The rectangular region at the very center that is separated diagonally into black and white sections reflects ratios ranging from about 0.6 to 1.6 and is about 11 arcsec square. The center of the PSF is the most crucial region for position estimation, so getting this part of the PSF wrong has serious consequences for astrometry, and of course also photometry.

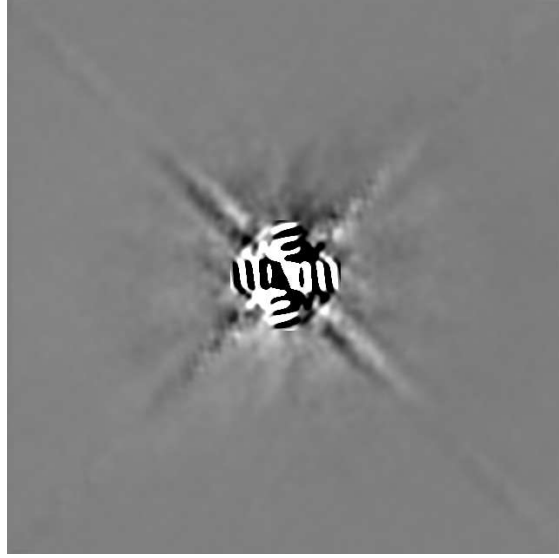


Figure 2. Difference image of W1 post-cryogenic PSFs in ascending vs. descending scans.

The structure revealed here has no impact on the measurements carried out by IPAC for *WISE* and *NEOWISE*, because those measurements are made on individual frames. The PSF structure is captured in the models, and the PSF orientation is always the same in the *WISE* frames. But this is not the case when using coadds in place of individual *WISE* frames.

Each epoch consists of ascending or descending scans exclusively for most tiles. so Therefore the PA averaging described above is done separately for ascending-scan epochs and descending-scan epochs for use in point-source extraction employing those different kinds of epoch exclusively, and these are then averaged together, weighted by epoch count, for use in point-source extraction employing all epochs.

For a given tile, option 0 uses PSFs averaged over the ascending and descending scan directions, and so these PSFs average over the differences shown here. Many tests were done comparing extracted point sources to those from AllWISE, and astrometric comparisons to other catalogs were also undertaken. At the same time, analysis of chi-squares showed that the error models were also not perfect, which was to be expected, because the PSF uncertainties were derived during WISE/NEOWISE calibration of raw image array data, not unWISE coadds, and the unWISE uncertainty images are

sample standard deviation images, not the product of WISE instrument calibration of effects such as dark-current subtraction, flat-fielding error, detector nonlinearity, etc.

This led to scale-factor, bias, and floor corrections to both the PSF and image uncertainties to bring the chi-squares into line. The PSF uncertainties mainly affect bright stars, and the image uncertainties mostly affect faint stars, and this separation allowed different corrections to be derived for the PSFs and the image uncertainties. Once these calibrations were done, the product being obtained from option-0 processing was scrutinized and found to be within the quality requirements of the project. But it was clear that splitting the extraction processing between ascending-only and descending-only scan directions should remove some of the residual errors due to the approximations in the direction-averaged PSFs.

3.3. *Detection*

Source detection for the preliminary CatWISE catalog was done simultaneously in W1 and W2 with the Multiband Detection (MDET) software used in the WISE pipeline (Marsh & Jarrett 2012). For the preliminary CatWISE catalog, the Image Co-addition with Optional Resolution Enhancement (ICORE) software (Masci 2013) was used to resample the 2048×2048 $2.^{\circ}75$ pixel NEO3 unWISE coadds to the 4095×4095 $1.^{\circ}375$ pixel detection image format used for WISE, using a PSF appropriate for each tile and band as the interpolation kernel. The PSF interpolation kernel smooths the images, providing a matched filter for optimal detection of isolated point sources. For uncertainties, the “std” unWISE images were used, which are the standard deviation at each pixel of the individual WISE exposures. An SNR threshold of 1.8 was selected, corresponding to a source reliability of 50% based on deeper Spitzer data.

At the high source densities typical for CatWISE in coadds of ~ 100 or more individual WISE exposures, this matched filter detection methodology yields an asymptotic number of $\sim 60,000$ detected sources per tile (or $\sim 25,000$ deg $^{-2}$, Figure 3) and hence becomes incomplete, particularly in W1. Schlafly et al. (2019) present an alternative approach (“crowdsouce”) which results in higher detected source densities, but does not provide motion estimates.

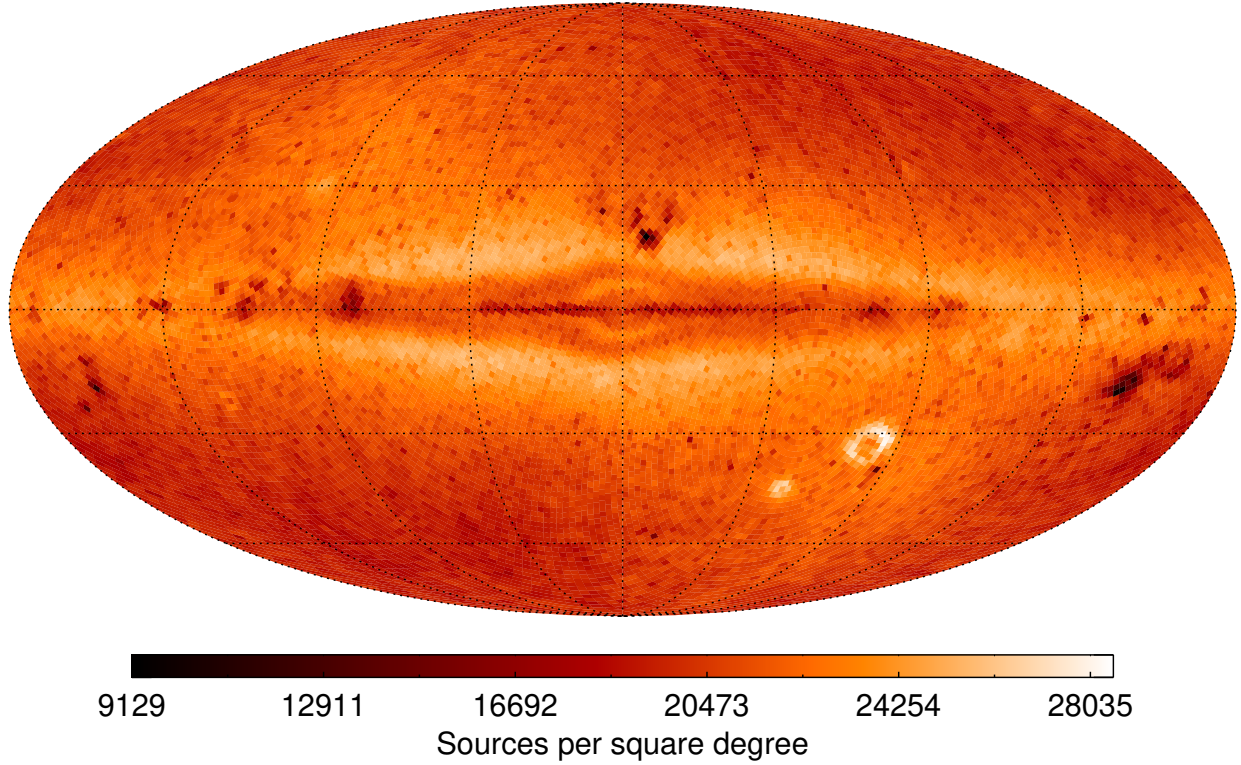


Figure 3. Map of CatWISE catalog source density in galactic coordinates.

3.4. Source Measurement

Source photometry, astrometry, and motion estimation for CatWISE use an adapted version of the WPHOT software developed for the AllWISE pipeline. For AllWISE, source positions detected in each coadded tile image were propagated to individual exposures, and the least-square best-fit to the psf for source position and flux were solved for. A linear motion is also solved for, based on the observation time of the images.

CatWISE did not have the computational resources to perform the source fitting on all of the many hundreds of individual exposures that contribute to a coadded tile image. Because the 12 exposures for a given inertial position in each sky coverage are obtained within less than two days, the motions of sources beyond the solar system can be assumed to be fixed for each sky coverage or "epoch." Therefore CatWISE ran WPHOT treating unWISE epoch coadd images as the individual images.

One other significant modification to the AllWISE WPHOT process was implemented for CatWISE. The WISE PSF is asymmetric in the survey scanning direction, which is along lines of ecliptic longitude (see e.g. Figure 2 in section IV.2.b.i of the NEOWISE Explanatory Supplement). Since the scan direction is similar for all individual images in an epoch coadd, the asymmetry with scan direction is preserved. The scan direction for a given inertial position alternates every 6 months, i.e. between epochs. WPHOT was not designed to use a time-dependent PSF, but with 8 or more epoch coadd images per position, CatWISE elected to measure source properties with WPHOT separately for the groups of four or more epoch coadds in each of the two scan directions, and then merge the two results. This “option 1” processing was done for all but the 50 tiles closest to the ecliptic poles, where a broad range of scan directions contributes to a coadded image, and a single WPHOT run was made.

3.5. *Astrometry*

The wphot routine developed for AllWISE and adapted for CatWISE carries out point-source extraction, solving for both photometry and astrometry simultaneously. The routine performs this solution assuming sources are inertially fixed (the “stationary fit”), and also searches for a solution assuming a linear motion with time (the “motion fit”). The χ^2 minimization fit can be performed at any location in the flux image. The goal of astrometry is to find the location at which χ^2 is at the bottom of a local minimum.

The stationary fit treats χ^2 as a function defined on a two-dimensional space right ascension (α) and declination (δ). As one moves around in the space, χ^2 decreases and increases as the local flux distribution appears more or less like a point source, i.e., like a flux-scaled PSF. In the vicinity of a real point source, χ^2 tends to be concave, although with some noise fluctuations. At any point, both χ^2 and its gradient can be calculated. The astrometry solution is found by searching along the opposite direction of the gradient until the gradient flattens out, i.e., the local minimum has been found. This is a standard numerical technique known as the gradient descent method. The (α, δ) where χ^2 is estimated to be minimal is the position assigned to the source, and the scale factor on the PSF that minimizes χ^2 there is the flux estimate. The value of χ^2 is recorded, as are the individual

χ^2 for the W1 and W2 flux fits. Standard Gaussian error analysis provides uncertainties for (α, δ) and flux, and standard formulas are applied to the flux and its uncertainty to obtain magnitudes and magnitude uncertainties. The error model includes both PSF error and image flux error.

The motion fit treats χ^2 as a function defined on a four-dimensional space, $(\alpha, \delta, \mu_\alpha, \mu_\delta)$, where μ_α and μ_δ are the angular motions in (α, δ) . As discussed below, one processing mode (called option 0) employs all epochs in a single execution of the photometry/astrometry program; in this case, the motions may include parallax effects, and so they are not true proper motions in general. The other processing mode (option 1) processes ascending scans and descending scans separately, and one result of the scan strategy is that except in the vicinity of an ecliptic pole, this separates the observations into opposite elongations, so that any measurable motions are a true proper motions.

The model used for the motion solution replaces the single location of the stationary solution with locations along a linear function of time. The slopes of this line in the (α, δ) directions are the motions (μ_α, μ_δ) .

More details may be found in the WISE All-Sky Release Explanatory Supplement: http://wise2.ipac.caltech.edu/docs/release/allsky/expsup/sec4_4c.html#satrad

3.6. Option 1 vs Option 0

Option 1 produces two independent source lists for a given tile, one extracted from unWISE epoch coadds constructed from ascending scans (Asce) and one from descending-scan epochs (Desc). These are merged into a single source list with refined parameter estimates as follows. Each source in each list has among its parameters an identifier of the detected source from the list input to the extraction program. This parameter is named mdetID. The Asce and Desc sources with the same mdetID were extracted for the same detection and are therefore apparitions of the same point source. A list of sources associated by mdetID is constructed for processing by the parameter estimate refinement program. The Asce and Desc sources are almost in perfect one-to-one correspondence, but a small number of mismatches occur because of active deblending in the extraction program. Active deblending is a process in which a new source (not from the detection program) may be inserted into the fitting region if the otherwise-best chi-square value is above a threshold and if inserting a new

source reduces the overall chi-square of the fit by a minimum required mount. Full details may be found in section IV.4.c of the *WISE* All-Sky Explanatory Supplement. The relevant point here is that active deblending may proceed differently in the Asce data and the Desc data. Actively deblended sources have the same mdetID, so when that is not unique, a nearest-match criterion is applied.. The number of Asce members may not equal the number of Desc members, so that some extractions are left over and discarded, leaving a one-to-one association list. Corresponding parameters in the list for each Asce-Desc source pair are combined in ways appropriate to the parameter type when the Asce and Desc apparitions have non-null values, otherwise the single non-null values are retained, if any. The combination method is generally straightforward for each type, e.g., various counters are simply summed. The handling for three types, however, should be mentioned in particular: aperture magnitudes, position coordinates, and template-fit magnitudes. Aperture magnitudes are computed from the same full-depth coadd in Asce and Desc, hence they are almost 100% correlated, differing only slightly in the position of the aperture centers. These magnitudes and their uncertainties are simply averaged without weighting. The (α, δ) vectors are averaged using inverse-covariance weighting. The averaging is done in a local Cartesian projection consistent with the uncertainty representation. A transformation matrix is defined as follows: starting with a Cartesian XYZ system whose Z axis points to the celestial north pole and whose X axis points to the vernal equinox, we perform two Euler rotations that place the new Z axis on the Asce celestial (α, δ) position with the Y axis aligned with the local north-south direction, and the X axis aligned with the local east-west direction, where by local we mean within a few arcseconds of the origin, since it is very rare for an extracted sources position to vary between the Asce and Desc solutions by more than that. We construct the vector to the Desc position in the original celestial coordinate system and transform it into the new system, wherein its X and Y offsets from the origin correspond to (α, δ) offsets of the Desc position from the Asce position. The offset vector is averaged with (0,0) using inverse covariance weighting to obtained the refined offset vector, which is then converted back to refined (α, δ) coordinates with uncertainties obtained via standard Gaussian estimation. The image pixel coordinates are then computed for the refined position using the unWISE coadd WCS information.

Template-fit photometry is refined by averaging the flux values using inverse-variance weighting. This yields refined flux values and reduced uncertainties that are used to recompute the magnitudes, magnitude uncertainties, and signal-to-noise ratios.

We compared the astrometric performances of Option 1 and Option 0 on a set of 19 known ultracool dwarfs, chosen from the literature. Our test set included extremely cold, very fast moving objects (e.g. WISE J085510.83–071442.5, $\mu_{\text{tot}} \sim 8 \text{ arcsec yr}^{-1}$; Luhman 2014), as well as warmer, slower M dwarfs (e.g. WISE J072003.20084651.2, $\mu_{\text{tot}} \sim 0.12 \text{ arcsec yr}^{-1}$; Scholz 2014). Option 1 proved superior, delivering good motion measurements for 17 out of the 19 test objects, while option 0 only recovered 13 out of the 19 test objects, with a clear drop in performance for objects with $\mu_{\text{tot}} \gtrsim 2.5 \text{ arcsec yr}^{-1}$ – only one out of the five fastest moving objects in our test sample is correctly measured by option 0, while option 1 measures four out of these five.

We note that the two objects that our pipeline is unable to correctly measure – WISE J163940.83–684738.6 and WISEPC J205628.90+145953.3 – are missed at the detection stage (Section 3.3) because they are partly blended with brighter nearby sources. These two sources were recovered when the detection step was run without the PSF filter, yielding reasonable motions, but they are not present in the delivered CatWISE catalog.

3.7. Artifact Flagging

Bright stars create a variety of scattered light effects and electronic-charge issues that require special handling by the software. These effects include scattered light halos, diffraction spikes, glints from off-frame bright stars, optical ghosting from internal reflections within the optical system, and charge persistence on the arrays. These can create false detections, hereafter called artifacts, or can contaminate detections of real, astrophysical sources. The goal of artifact flagging is to label spurious or affected sources so that the user can easily create source lists for which most of these problems are eliminated.

CatWISE employs two types of artifact flagging. One is the *cc_flags* values copied directly from AllWISE processing. If an AllWISE source is found within 2''.75 of a CatWISE source, this *cc_flag* is appended to the CatWISE source itself; if no AllWISE source is found within this radius, then

cc_flags contains a null value. These *cc_flags* values indicate whether a source is thought to be a real artifact (encoded as an upper-case letter) or a real source contaminated by an artifact (encoded as a lower-case letter). Each band is flagged separately, and since AllWISE processing included data in all four WISE bands – W1, W2, W3, and W4 – the *cc_flags* value is a four-character string. The possibilities are “0” for no artifact or contamination, “D” or “d” for a diffraction spike, “H” or “h” for a scattered light halo, “O” or “o” for an optical ghost, or “P” or “p” for charge persistence². A more detailed description can be found in section IV.4.g of the WISE All-Sky Explanatory Supplement³. For a CatWISE source having multiple AllWISE sources within the 2''.75 radius, the most pessimistic value per band is retained, as described in section 3.7.1 below.

The second type of artifact flagging, inherited from unWISE processing, is called *ab_flags*. One advantage of *ab_flags* is that these values are determined for every CatWISE source. The disadvantage is that *ab_flags* offer no information to distinguish between an outright artifact and a real astrophysical source that suffers from some level of artifact contamination. However, we have adjusted the flagging (section 3.7.3) so that only egregious artifacts – that is, spurious detections – are flagged. To be kept parallel with the logic of *cc_flags*, the *ab_flags* thus contain only upper-case letters “D”, “H”, “O”, or “P” or the value “0”. Furthermore, because the CatWISE data deal only with W1 and W2 data, the *ab_flags* values are only two characters long. Additional details are given in section 3.7.2.

These *cc_flags* and *ab_flags* values should be regarded as two different yet complementary methods for tagging sources of special concern to the user. As described in the WISE All-Sky Explanatory Supplement⁴, the *cc_flags* are known to overflag; their purpose is to produce a reliable catalog of source extractions free of contamination by artifacts, but they do so at the expense of completeness. To provide a complement to the *cc_flags*, the *ab_flags* are used to tag only the most egregious artifacts, thereby emphasizing completeness, albeit at the expense of reliability. Users of the CatWISE data products can thus query against these two sets of artifact flags to best fit their needs.

² Glints are rarely seen in coadds, so their effects are not flagged in CatWISE data.

³ http://wise2.ipac.caltech.edu/docs/release/allsky/expsup/sec4_4g.html

⁴ http://wise2.ipac.caltech.edu/docs/release/allsky/expsup/sec4_4g.html

3.7.1. Setting the *cc_flags* Values When There are Multiple Matches

The values of *cc_flags* are taken directly from a join of the AllWISE Point Source Catalog and Reject Table. When more than one of these AllWISE sources matches to within 2''.75 of a CatWISE source, the band-by-band *cc_flags* value of the CatWISE source is determined as follows. If there is an upper-case letter for any matching source, it takes precedence over any lower-case letter. The letter “D” is the highest priority followed, in order, by “P”, “H”, and “O”. If there are no upper-case letters for any matching source, lower-case letters have the next highest priority, in the same order (“d”, “p”, “h”, and “o”). If all matching sources have a value of “0” in that band, then “0” is used.

3.7.2. Translating the unWISE Bit Mask Values to *ab_flags*

The unWISE bit mask values at the (x,y) pixel location of the source are used to set the value of *ab_flags*, as shown in Table 1. A full description of the native unWISE mask bit meanings is available through the unWISE Catalog data release website⁵. Note that the checks against MASKB21 and MASKB22 are to ensure the the bright star itself is not flagged as either a diffraction spike or scattered light halo.

Table 1. Logic Used in Converting unWISE Bitmask Values to *ab_flags* Values

Value	Band	Logic
(1)	(2)	(3)
“D”	W1	MASKB0 or MASKB1 or MASKB7 or MASKB27 or MASKB29 but only if not MASKB21
...	W2	MASKB2 or MASKB3 or MASKB8 or MASKB28 or MASKB30 but only if no. MASKB22
“H”	W1	MASKB23 but only if not MASKB21
...	W2	MASKB24 but only if not MASKB22
“O”	W1	MASKB25 or MASKB26

Table 1 continued on next page

⁵ http://catalog.unwise.me/files/unwise_bitmask_writeup-03Dec2018.pdf, see Table 1.

Table 1 (*continued*)

Value	Band	Logic
(1)	(2)	(3)
<hr/>		
...	W2	MASKB11 or MASKB12
"P"	W1	MASKB13 or MASKB14 or MASKB17 or MASKB18
...	W2	MASKB15 or MASKB16 or MASKB19 or MASKB20

3.7.3. Adjusting the *ab_flags* Values

For the *ab_flags*, we performed by-eye checks over a small handful of selected tiles to make sure that the extent of the flagging matched expectations. These included tiles at range of Galactic latitudes. Several iterations were performed, primarily to tweak the extent of the halo flagging, before values were finalized. Figure 3 shows examples of these final checks in tiles containing 47 Tucanae (0048m727, $b = -44^\circ$), a portion of the Hyades (0657p151, $b = -24^\circ$), the COSMOS field (1497p015, $b = +41^\circ$), and Barnard's Star (2688p045, $b = +15^\circ$). Note that the upper-case *cc_flags* slightly overflag, as designed, particularly in scattered light halos.

3.8. Primary Flagging

WISE tiles, and, therefore, unWISE coadds, overlap each other by $180''$ on the equator. As a result, sources appearing near the edge of a tile will be detected in neighbouring tiles too. To flag and remove duplicate apparitions we adopted a pure geometric approach, equivalent to that adopted in [Schlafly et al. \(2019\)](#).

3.9. The Preliminary CatWISE Catalog

Preliminary CatWISE catalog sources are required to:

- 1) be "primary" in their tile (i.e. be from the tile where that source is furthest from the tile edge) and

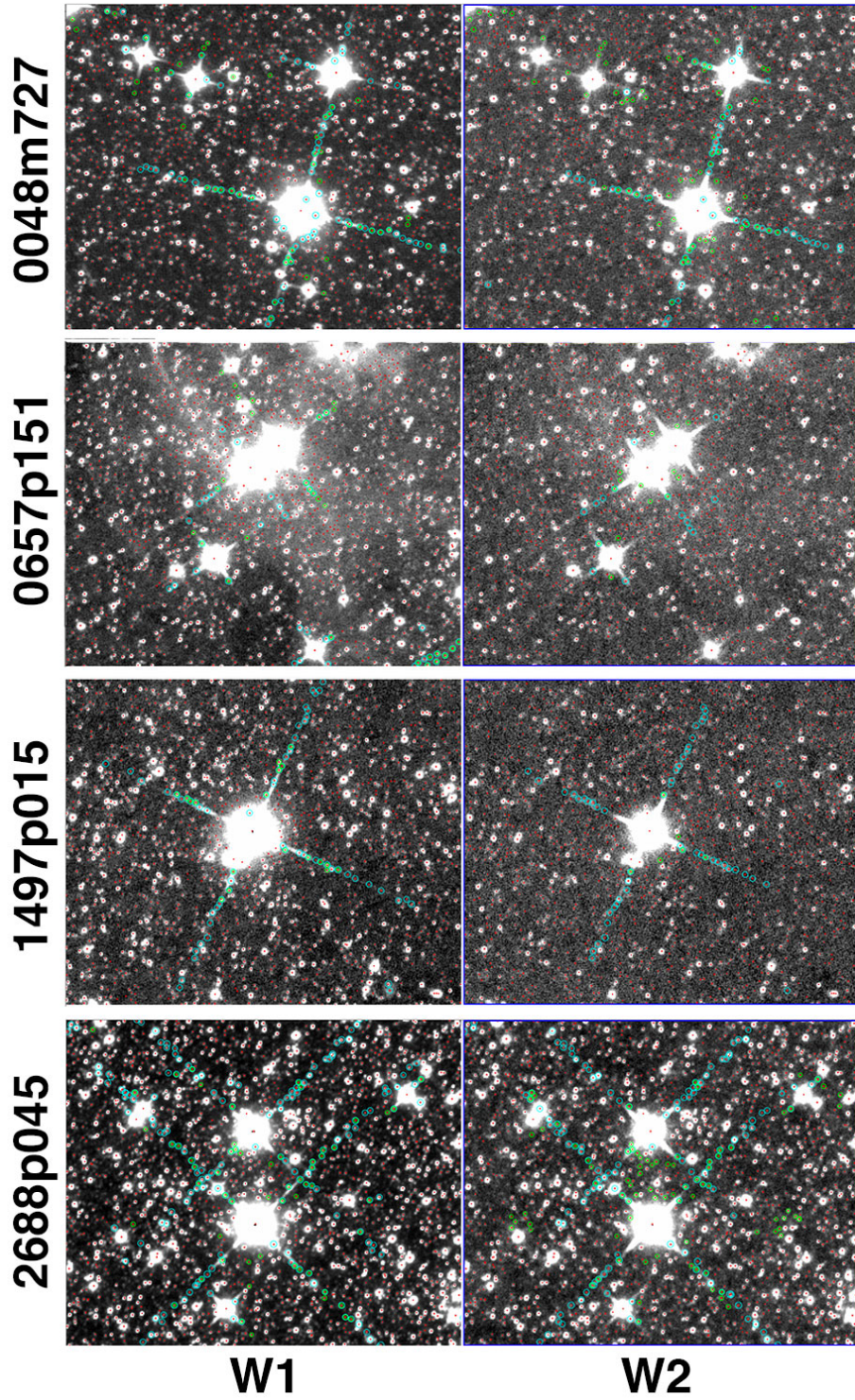


Figure 3. Each row shows W1 (left) and W2 (right) cutouts of tiles whose names are given along the far left. Detected CatWISE sources are shown by the red markers. Sources with upper-case *cc_flags* are circled in green and sources marked as artifacts by *ab_flags* are circled in cyan. Zoom in for details.

2) have W1 SNR ≥ 5 with no identified artifacts (a value of 0 for the "ab_flags" in the W1 part (left character) of column 178)

or

have W2 SNR ≥ 5 with no identified artifacts (a value of 0 for the "ab_flags" in the W2 part (right character) of column 178).

There are 957,285,574 sources that meet these criteria. The 111,394,986 that fail to meet these criteria go into the reject file for their tile. Reject files typically contain a few thousand sources. There are 186 formatted columns of information about each catalog source. Reject files have one additional column, indicating if the source is "primary" in its tile. Additional information about most of the columns is available via the AllWISE Explanatory Supplement.

4. ANALYSIS

4.1. Astrometry

We tested the astrometric performance of CatWISE against *Gaia* DR2 (Gaia Collaboration et al. 2018; Lindegren et al. 2018). We chose a test set of 141 tiles, sampling a wide range of Galactic latitude (b), source density, and ecliptic latitude (β). Table 2 lists a subset of 7 out of the 141 tiles used, with their relevant properties. These 7 were chosen to sample the full b range from the South Galactic Pole to the Galactic Center, along the $l = 0^\circ$ meridian, plus the north Ecliptic pole, the South Ecliptic pole, and the tile containing the COSMOS field. Figure 4–6 shows the position and motion precision. For the comparison, we cross-matched CatWISE to *Gaia* using a two-step matching. First, we searched for *Gaia* counterparts to CatWISE sources using a broad 20" matching radius, and retained all matches. Then, we used *Gaia* astrometry to move the *Gaia* putative counterparts to the CatWISE epoch, and repeated the match with a narrower 2.75" radius (corresponding to 1 pixel in the unWISE coadds), retaining only the closest *Gaia* source for each CatWISE object.

We then binned the matching sources in 0.5 mag bins and computed the standard deviation between the CatWISE and *Gaia* position and motion (shown by the red points in Figure 4–7), as well as the

median CatWISE motion uncertainties. For the position analysis, we used the *Gaia* positions moved at the epoch of the CatWISE measurements in the catalog).

We define ten metrics to characterize the astrometric performance of CatWISE:

- σ_{\min} and $\sigma_{\mu, \min}$ are the precision floor for positions and motions, respectively. These precision floors are determined as the median dispersion with respect to *Gaia* in the $8 < W1, W2, < 10$ mag interval, except at low Galactic latitude ($|b| < 10^{\circ}$) where we restrict to the $8 < W1, W2, < 9$ mag since the astrometric precision starts deteriorating significantly beyond $W1, W2 \sim 9$ mag (see e.g. Figure 4–6).
- $W1_{\min}$, $W2_{\min}$, $W1_{\mu, \min}$, and $W2_{\mu, \min}$ are the $W1$ and $W2$ mag at which σ_{\min} and $\sigma_{\mu, \min}$ are exceeded by no more than 20 mas and 5 mas yr $^{-1}$, respectively.
- $W1_{500}$ and $W2_{500}$ are the $W1$ and $W2$ mag at which the precision on coordinates reaches 500 mas.
- $W1_{\mu, 100}$ and $W2_{\mu, 100}$ are the $W1$ and $W2$ mag at which the precision on motion reaches 100 mas yr $^{-1}$.

The results for a subset of 7 representative tiles out of the 141 chosen as test sample are summarized in Table 3, while in Figure 8 and 9 we plot the results for the full test sample as a function of b and β respectively. We omit the results as a function of source density since all reported metrics do not show clear dependence on it.

σ_{\min} and $\sigma_{\mu, \min}$ are encouragingly small, on the order of 40 mas and 7 mas yr $^{-1}$, respectively. There is little dependence of both metrics on $|b|$ until $|b| < 5$, where they sharply rise towards their peak values of ~ 580 mas and ~ 22 mas yr $^{-1}$.

The plots of $W1_{\min}$, $W2_{\min}$, $W1_{\mu, \min}$, and $W2_{\mu, \min}$ shows strong dependence on $|b|$, with accelerating rise in brightness at lower $|b|$. At high b $W1_{\min}$ and $W2_{\min}$ are ~ 13 mag, while $W1_{\mu, \min}$ and $W2_{\mu, \min}$ are ~ 13.5 mag. All metrics rise to ~ 8 mag near the Galactic center.

$W1_{500}$, $W2_{500}$, $W1_{\mu, 100}$ and $W2_{\mu, 100}$ are ~ 17 mag down to $|b| = 20$. For tiles at lower b most $W1_{\mu, 100}$ and $W2_{\mu, 100}$ measurements are upper limits only (open triangles). This is a consequence of the fact

Table 2. CatWISE Astrometric Performance Fields Performance

Tile	l	b	β	Exp	#	Comment
0133m258	139.6	-88.6	-28.8	106	61294	SGP
0890m667	52.9	11.0	15.1	7154	71462	SEP
1497p015	27.3	12.5	17.0	90	58961	COSMOS
2657m288	-0.2	0.6	-5.4	86	63368	GC
2709p666	96.4	-30.2	89.6	7839	61702	NEP
2777m349	-0.6	-11.4	-11.6	81	58911	
3195m425	-1.2	-44.4	-25.4	99	57928	

Table 3. CatWISE Astrometric Performance

Tile	Coordinates					Motion				
	σ_{\min}	W1 _{min}	W1 ₅₀₀	W2 _{min}	W2 ₅₀₀	$\sigma_{\mu, \min}$	W1 _{μ, \min}	W1 _{$\mu, 100$}	W2 _{μ, \min}	W2 _{$\mu, 100$}
	mas	mag	mag	mag	mag	mas yr ⁻¹	mag	mag	mag	mag
0133m258	31.9	12.5	17.2	12.5	17.0	7.5	13.5	16.9	13.5	16.7
0890m667	52.9	11.0	15.1	11.0	15.0	7.4	14.5	18.2	14.5	>20.5
1497p015	27.3	12.5	17.0	12.5	16.8	8.5	13.5	16.8	13.5	16.7
2657m288	526.4	8.0	8.4	8.0	8.3	22.2	9.0	>11.0	9.0	>11.5
2709p666	37.7	12.0	18.5	12.0	19.0	7.3	15.5	>19.0	15.5	>20.0
2777m349	32.1	10.5	14.3	10.5	14.4	7.0	12.0	15.9	12.0	15.8
3195m425	27.8	12.5	17.2	13.0	17.2	6.5	13.5	16.9	13.5	16.8

that at lower $|b|$ CatWISE only detects brighter sources because of confusion noise, and the motion uncertainties never reach the 100 mas yr⁻¹ level. These metrics show a slight dependence on ecliptic latitude, as expected given the deeper coverage at high β .

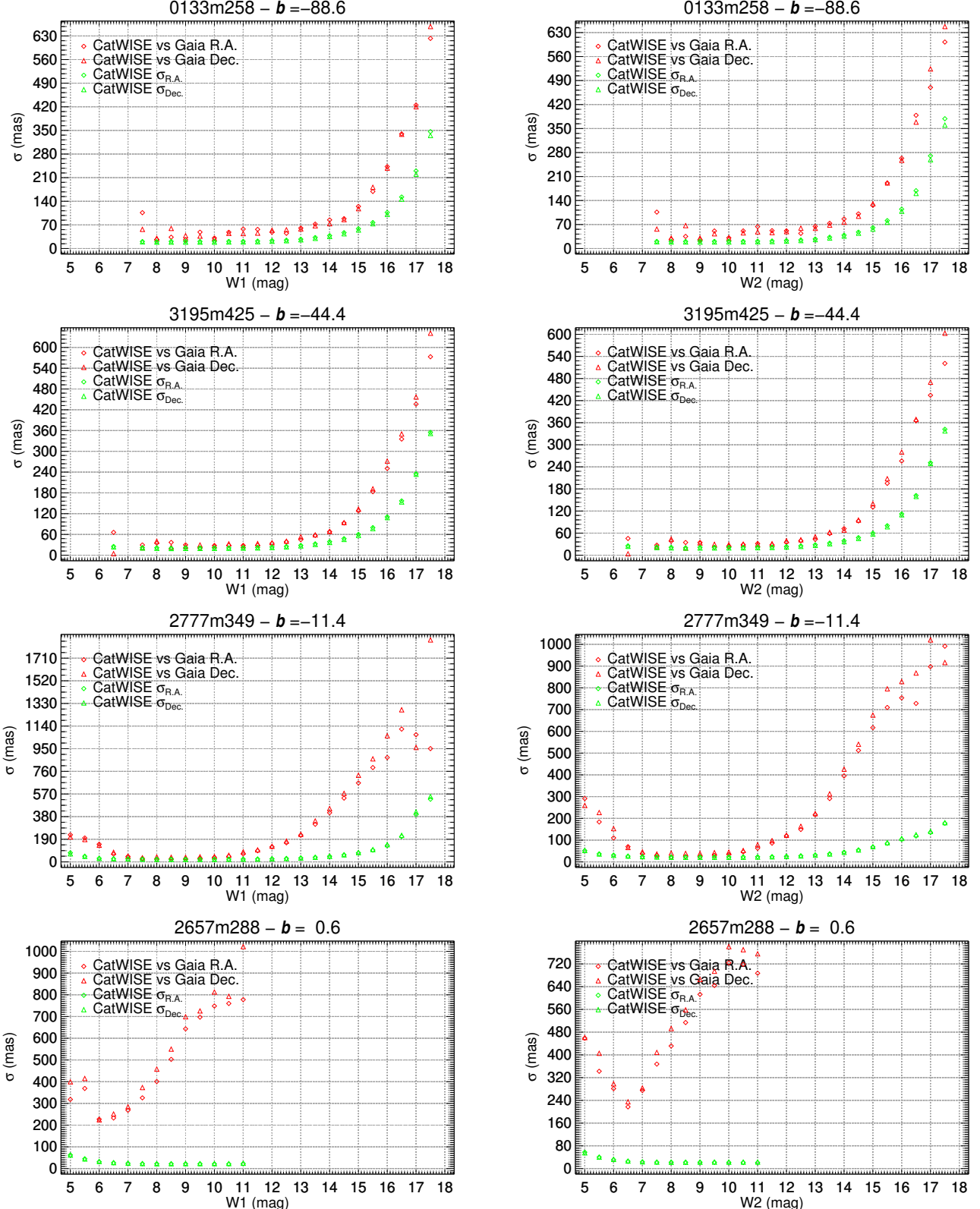


Figure 4. Comparison of CatWISE astrometry against *Gaia* DR2 in four tiles spanning the southern Galactic hemisphere, from the Galactic South Pole (tile 0133m258, top panels) to the Galactic Center (tile 2657m288, bottom panels). The standard deviation between CatWISE position measurements and *Gaia* DR2 position measurements, in 0.5 mag bins, is shown in red. Green points are the median CatWISE uncertainties in the same 0.5 mag bins.

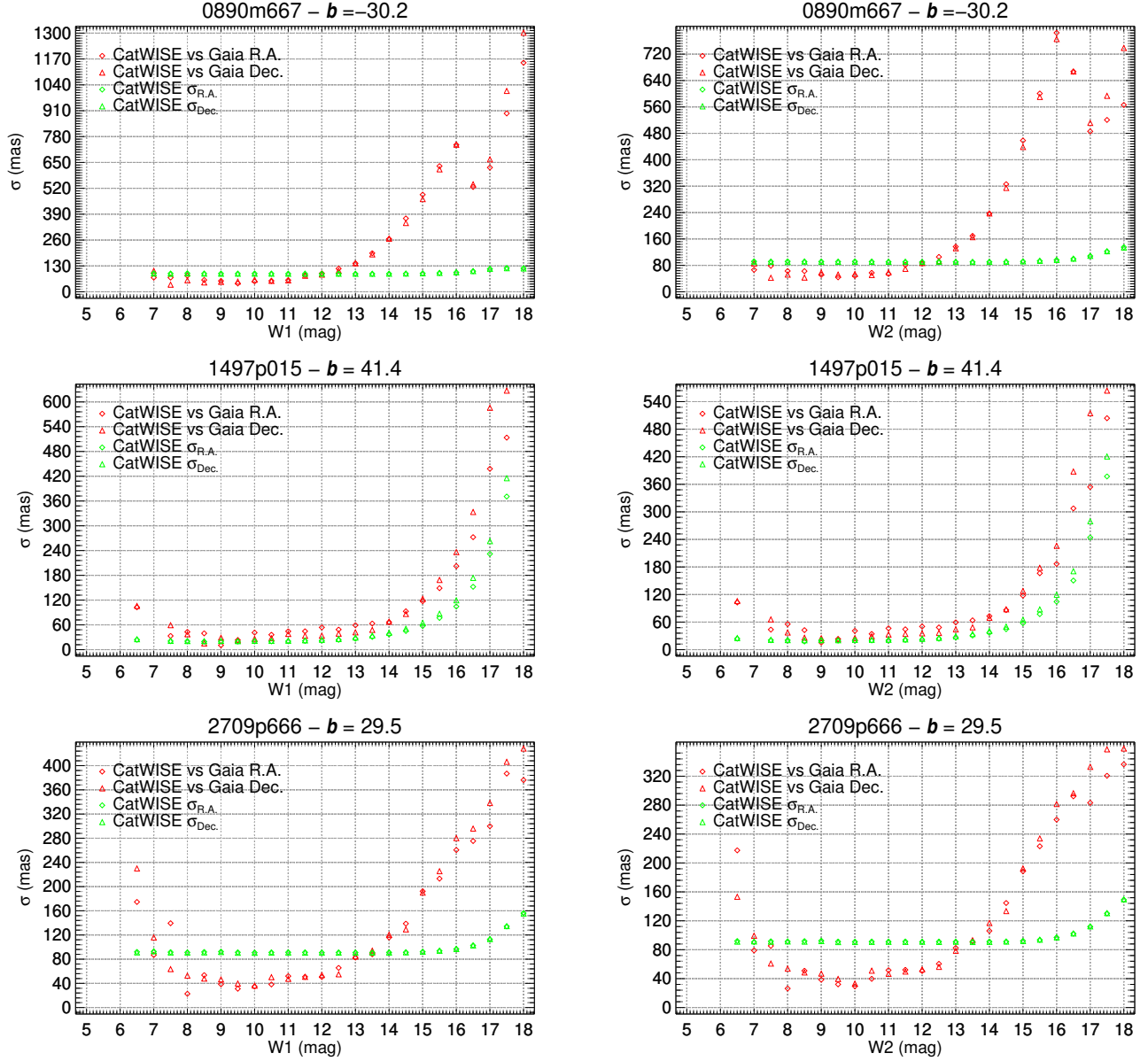


Figure 5. Same as Figure 4, but for the tile containing the South Ecliptic Pole (0890m667), COSMOS (1497p015), and the North Ecliptic Pole (2709p666).

4.2. Photometry

TO BE SUPPLIED

5. SCIENCE

TO BE SUPPLIED

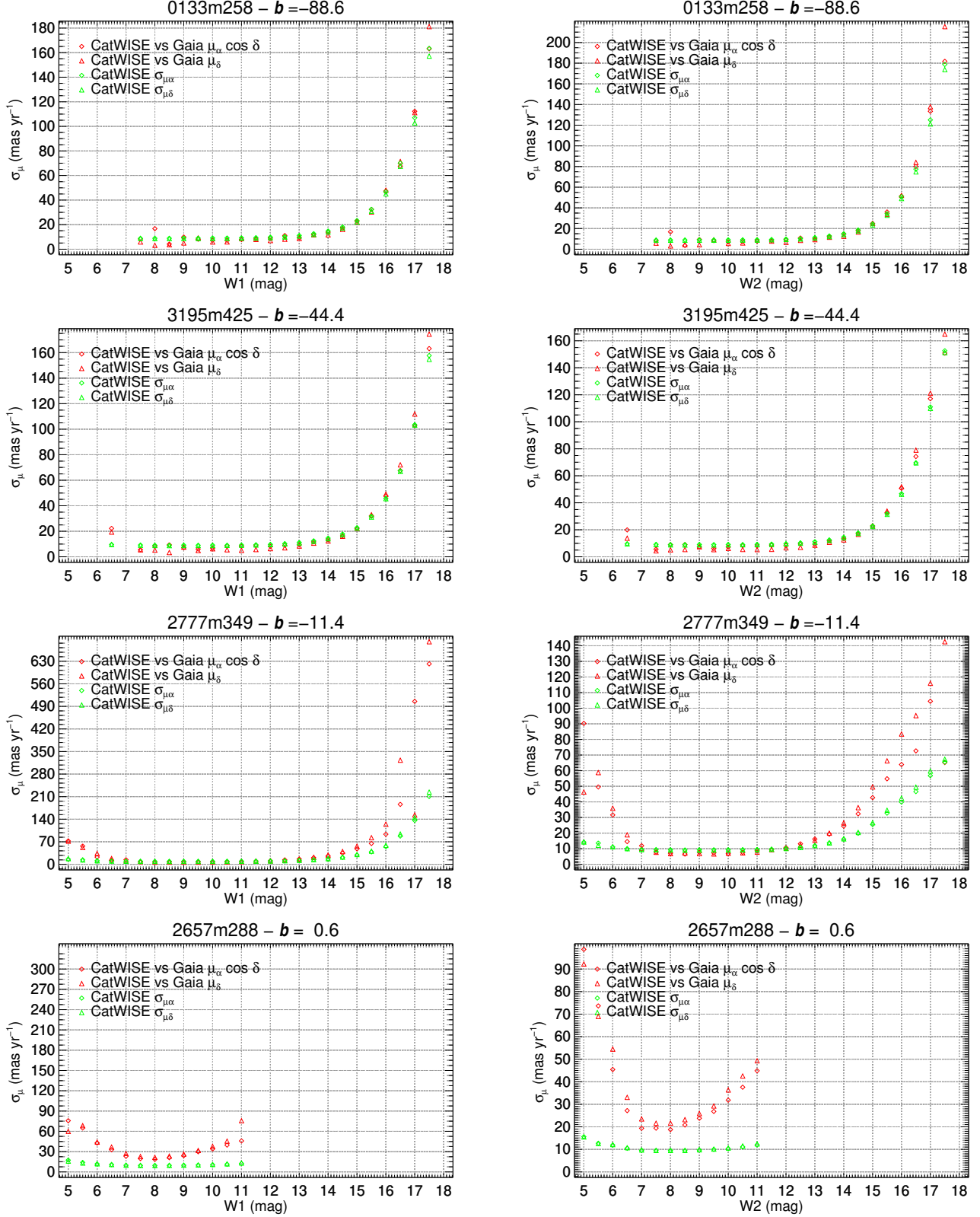


Figure 6. Same as Figure 4, but for motion measurements.

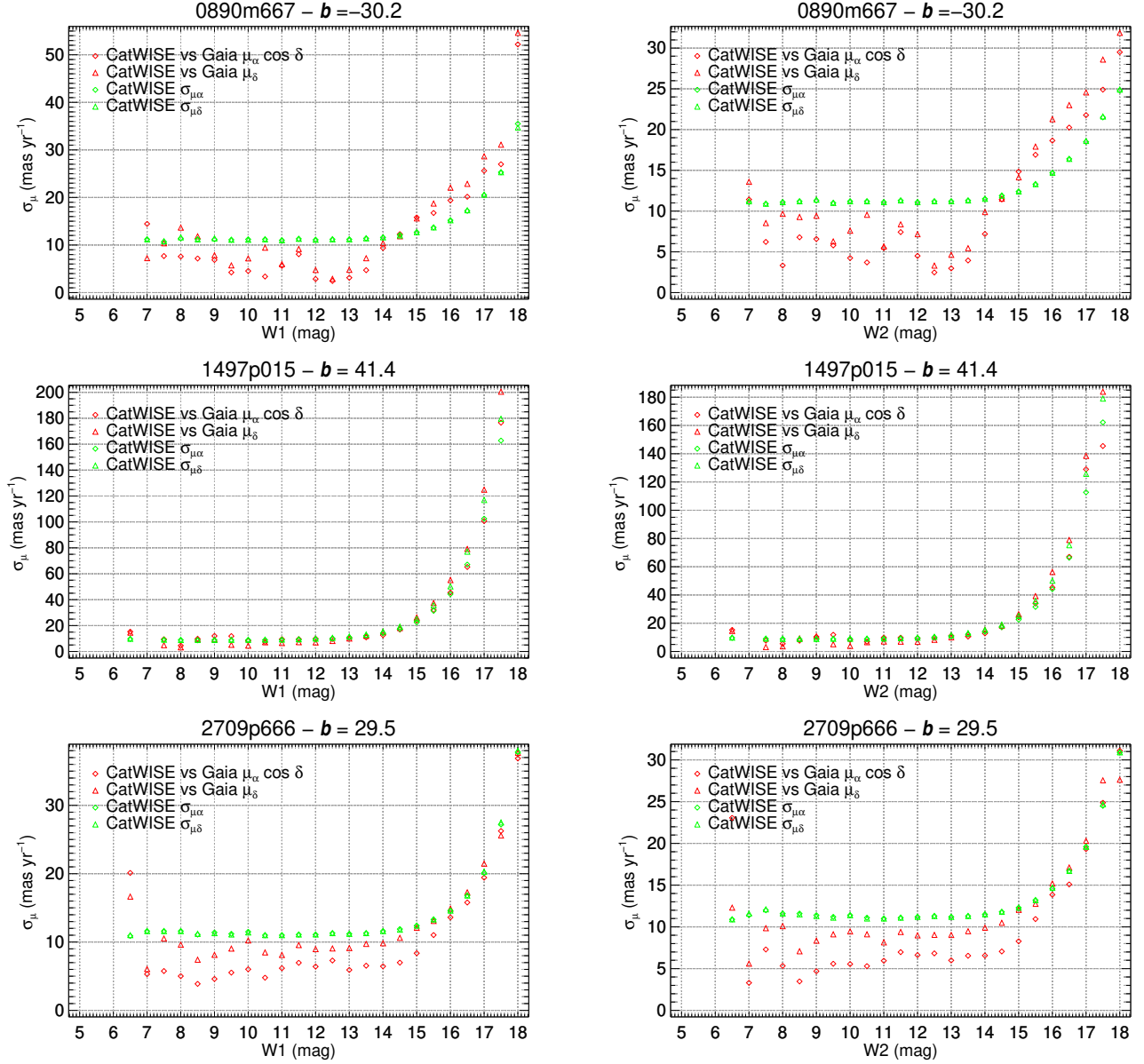


Figure 7. Same as Figure 6, but for the tile containing the South Ecliptic Pole (0890m667), COSMOS (1497p015), and the North Ecliptic Pole (2709p666).

6. DATA ACCESS

Current information about CatWISE data products is provided at <https://catwise.github.io>. The CatWISE catalog and reject files have been transferred to a data repository at the National Energy Research Scientific Computing Center (NERSC). The files were also transferred to the Infrared Science Archive (IRSA), where the individual tile files were merged into the IRSA database.

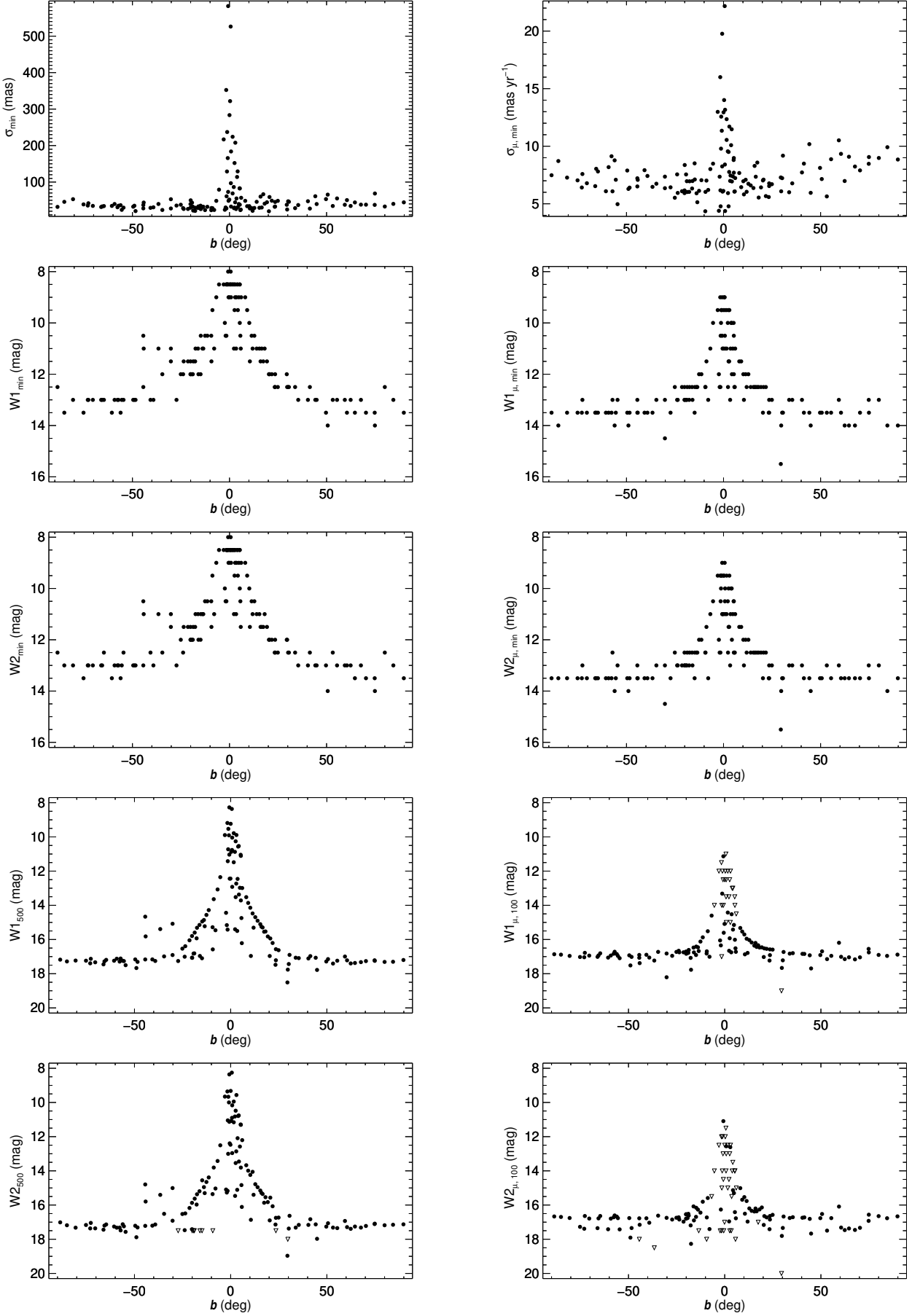


Figure 8. Astrometric performance of CatWISE as a function of Galactic latitude

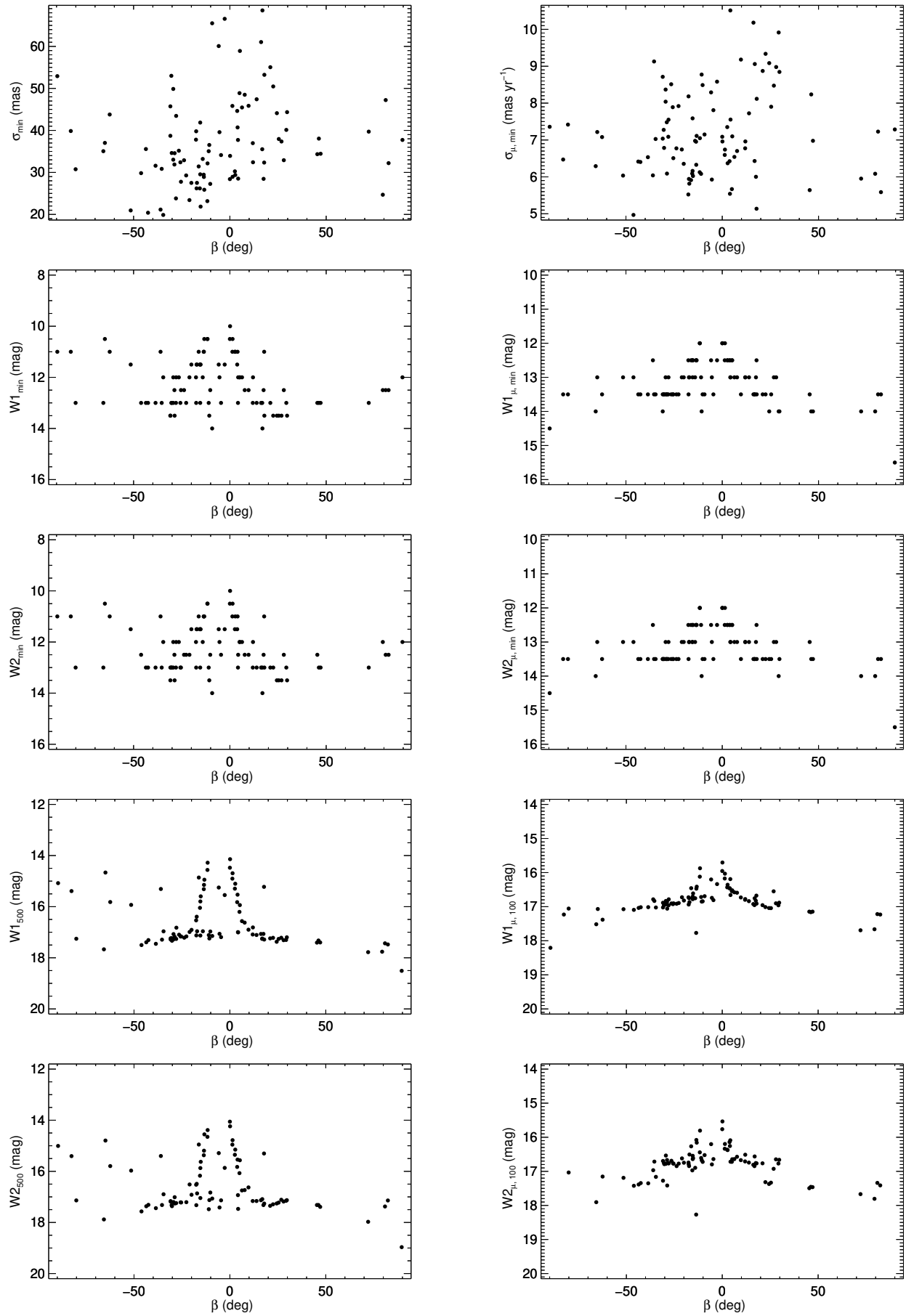


Figure 9. Astrometric performance of CatWISE as a function of Ecliptic latitude

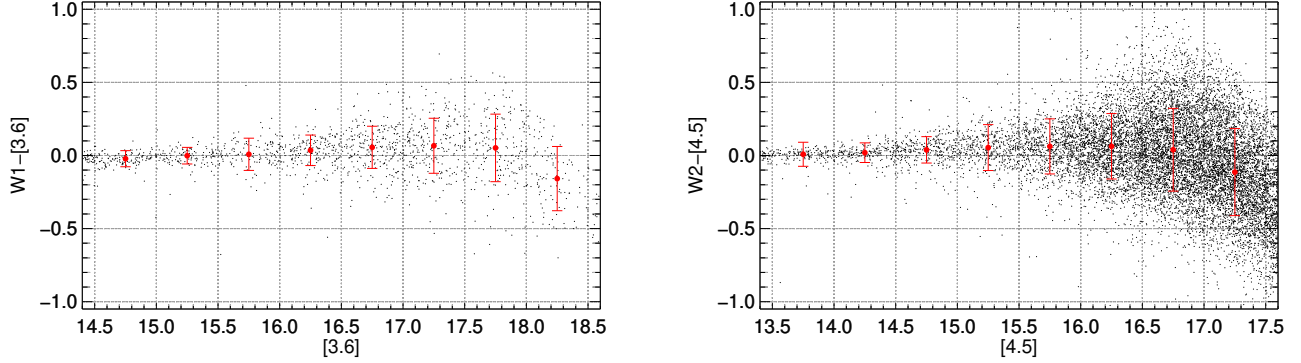


Figure 10. Comparison of CatWISE photometry to *Spitzer* photometry for COSMOS. **Left:** Difference between CatWISE W1 PSF and *Spitzer* S-COSMOS 2.9 radius aperture photometry at [3.6], for sources with $-0.1 < [3.6] - [4.5] < 0$ and $< 10\%$ flux increase from the 1.9 to 2.9 aperture. Mean differences and standard deviations in 0.5 mag bins are shown by the red points and error bars. **Right:** The analogous comparison for CatWISE W2 and *Spitzer* [4.5] photometry, but without the restriction on *Spitzer* source color.

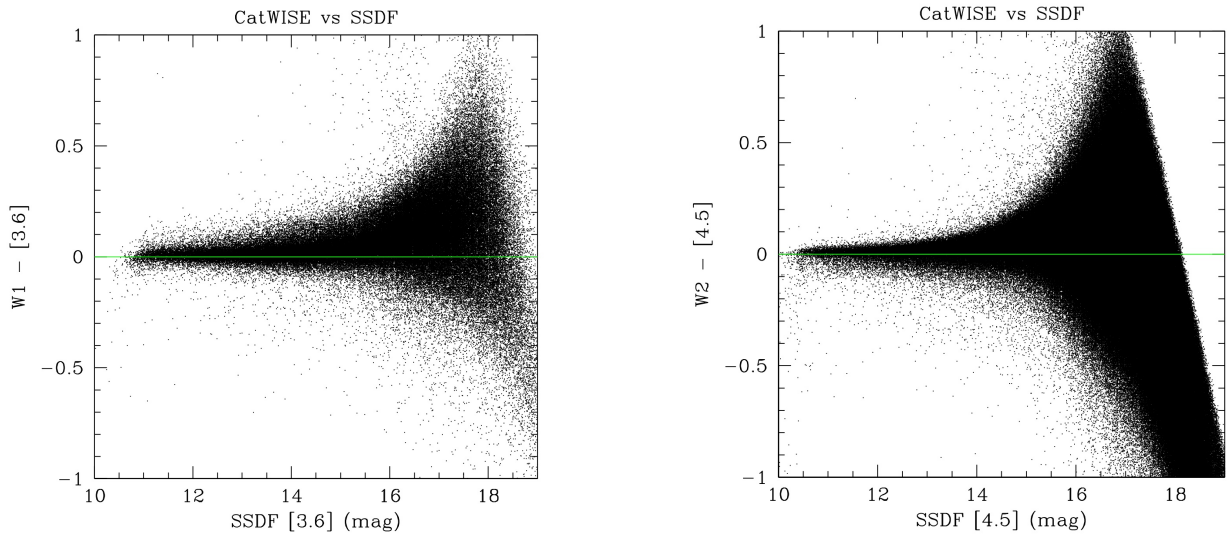


Figure 11. Comparison of CatWISE photometry to *Spitzer* photometry for SSDF.

The Preliminary CatWISE catalog became publicly accessible on 2019 May 14 at
<https://portal.nersc.gov/project/cosmo/data/CatWISE/prelim>
in 18,240 pairs of gzipped ascii files (one catalog and one reject file per tile) in IPAC table format, organized into 359 directories, one for each decimal degree of right ascension from 0 to 358

(there are no tiles beginning with 359). The catalog will also soon become available from IRSA (<https://irsa.ipac.caltech.edu>) as a contributed data set.

CatWISE uses data products from WISE, which is a joint project of the University of California, Los Angeles, and the Jet Propulsion Laboratory (JPL)/California Institute of Technology (Caltech), funded by the National Aeronautics and Space Administration (NASA), and from NEOWISE, which is a JPL/Caltech project funded by NASA. Characterization of CatWISE performance uses data from Gaia and from Spitzer. CatWISE is led by JPL/Caltech, with funding from NASA's Astrophysics Data Analysis Program (ADAP), and is also supported in part by ADAP grant NNH17AE75I at Lawrence Berkeley Laboratory. CatWISE is also supported by the Fellowships and Internships in Extremely Large Data Sets (FIELDs) program funded by NASA at UC Riverside. FM is supported by an appointment to the NASA Postdoctoral Program at the Jet Propulsion Laboratory, administered by Universities Space Research Association under a contract with NASA.

REFERENCES

- Caselden, D., Westin, P., Meisner, A., et al. 2018, ASCL:1806.004.
- Connors, M., Wiegert, P., & Veillet, C. 2011, Nature, 475, 481
- Cutri, R. M., Wright, E. L., Conrow, T., et al. 2012, Explanatory Supplement to the WISE All-Sky Data Release Products, <http://wise2.ipac.caltech.edu/docs/release/allsky/expsup>
- Cutri, R. M., Wright, E. L., Conrow, T., et al. 2013, Explanatory Supplement to the AllWISE Data Release Products, <http://wise2.ipac.caltech.edu/docs/release/allwise/expsup>
- Cutri, R. M., Mainzer, A., Conrow, T., et al. 2015, Explanatory Supplement to the NEOWISE Data Release Products, <http://wise2.ipac.caltech.edu/docs/release/neowise/expsup>
- Gaia Collaboration, Brown, A. G. A., Vallenari, A., et al. 2018, A&A, 616, A1.
- Jarrett, T. H., Cohen, M., Masci, F., et al. 2011, ApJ, 735, 112
- Lang, D. 2014, AJ, 147, 108
- Lindgren, L., Hernández, J., Bombrun, A., et al. 2018, A&A, 616, A2
- Luhman, K. L. 2013, ApJL, 767, L1
- Luhman, K. L. 2014, ApJL, 786, L18

- Marsh, K. A., & Jarrett, T. H. 2012, PASA, 29, 269
- Masci, F. 2013, arXiv:1301.2718
- Mainzer, A., Bauer, J., Grav, T., et al. 2011, ApJ, 731, 53
- Mainzer, A., Bauer, J., Cutri, R. M., et al. 2014, ApJ, 792, 30
- Meisner, A. M., Lang, D., & Schlegel, D. J. 2018a, RNAAS, 2, 1
- Meisner, A. M., Lang, D., & Schlegel, D. J. 2018b, AJ, 156, 69
- Meisner, A. M., Lang, D., & Schlegel, D. J. 2018c, RNAAS, 2, 202
- Schlafly, E. F., Meisner, A. M., & Green, G. M. 2019, ApJS, 240, 30
- Scholz, R.-D. 2014, A&A, 561, A113
- Tsai, C.-W., Eisenhardt, P. R. M., Wu, J., et al. 2015, ApJ, 805, 90
- Wright, E. L., Eisenhardt, P. R. M., Mainzer, A. K., et al. 2010, AJ, 140, 1868